Design and Simulation of Grid-Connected Photovoltaic System's Performance Analysis with Optimal Control of Maximum Power Point Tracking MPPT Based on Artificial Intelligence

Faouzi Didi[1], Moustafa Sahnoune Chaouche[1], Malika Amari[1], Ameur Guezmir[2], Kamel Belhenniche[4], Abdelhamid Chellali[3]

1LERM - Renewable Energy and Materials Laboratory. Department of Common-Core, Faculty of Technology. University of Médéa , 26.000, Algeria

2 Laboratory of Magnetic materials (LMM), University of Djillali Liabes , Sidi-Bel Abbes BP 89, 22000.

3Laboratory of Biomaterials and Transport Phenomena (LBMPT).

4Faculty of Technology, Department of Common-Core Technology, University of Médéa , 26.000, Algeria.

(+ Corresponding author)

Contribution/Originality: The paper's primary contribution is in finding the most appropriate model that treats the problem of MPPT of grid-connected photovoltaicto achievemaximum power - using four techniques of artificial intelligence.

Received : 11-09-2022 **Accepted** : 03-01-2023 **Published** : 27-03-2023

Abstract

The research presented in this paper is part of a more significant effort to improve the dynamic and static performance of power generation systems using solar panels under specific climatic conditions. The solar panel can produce the greatest power only at the specified voltage and electric current levels. Environmental variables, such as random atmospheric oscillations, have a significant effect on the performance of a solar system connected to the network. Irradiation and ambient temperature are the two inputs to a PV (photovoltaic) system. Because solar radiation varies in nature, the PV system efficiency is low. To improve the efficiency of a solar PV system, several maximum power point tracking (MPPT) approaches are used. The purpose of this paper is to improve the performance of DC/DC chopper controllers and PV inverters in the face of abrupt climate change. To that end, the primary goal of this paper is to compare the following maximum power point search (MPPT) algorithms: the incremental conductance (IC) algorithm, the fuzzy logic (FL) algorithm, VSI controller, and the particle swarm optimization (PSO)

strategy. These algorithms wereevaluated in terms of efficiency, stability, and speed. A 100 kW PV system is design usingMATLAB software 2021a version.
Keywords: Modeling, PSO algorithm, PVsystem, Grid connected PV, MPPT control, Fuzzy controller, VSI control, IC algorithm.

Tob Regul Sci. ™ 2023;9(1): 1074-1098
DOI: doi.org/10.18001/TRS.9.1.73

Introduction

Grid-connected PV systems are of tremendous interest for producing power in large-scale applications because of their economically optimal size, design, and cost [1, 2].The photovoltaic energy sector saw tremendous progress in the last decade. As a result of this progress, complex PV grid topologies have begun to evolve to boost power, efficiency, and reliability. Furthermore, grid-connected PV systems (which do not require batteries) are well-known for being less expensive than stand-alone PV systems (which do require batteries)[3]. Despite significant advancements in the field of PV systems, there are still issues with PV grids such as voltage regulation, power quality, and grid problems. A PV grid requires a robust control mechanism to mitigate all of these drawbacks [4, 5].

The maximum power point tracking (MPPT) controller was created to deal with the strains caused by various environmental fluctuations[5, 6]. This controller's performance is determined by how soon it reaches 1000MPPT, how well it oscillates around that point, and how resistant it is to abrupt atmospheric changes. The MPPT technique recently attracted a lot of attention as a way to improve the dynamic performance of PV systems, particularly in terms of tracking the MPPT in the presence of various local maxima during the night[5, 7]. Among the options found in the literature, there is a proposal to reconfigure the structure to reduce shading by providing an optimal PV system configuration to achieve the MPPT. To identify the shadowed PV module and minimize power losses, Tabanjat, et al. [8] suggested a method based on fuzzy logic (FL) with the online reconfiguration solution[5, 6]. To define likely connection architectures, Parlak [9] proposed a configuration digitization algorithm. This method solely employs short-circuit currents to produce PV modules from the same photovoltaic branch with current values that are close to those of a short-circuit [9]. Under uniform lighting conditions, traditional MPPT approaches such as incremental conductance (IC) produce good results [8]. However, because the P-V curve has numerous peaks, this performance is not guaranteed during outperforms OP. As a result, the local maximum could trap ICTan, et al. [7]; Lyden and Haque [10]. Sai, et al. [11]suggested a method for drawing the I(V) curve without disrupting the functioning of a PV system. Other studies have usedMPPT techniques based on artificial intelligence; among these research studies, Nedjma [6]used the FL-based MPPT algorithm. The simulation results showed

that the suggested technique outperforms the perturbation and observation (P&O) algorithm in terms of dynamic reaction capacity and speedresponseunderdifferentcircumstances [12-13]. Another form of MPPT technology, based on the metaheuristic approach, has piqued the curiosity of researchers.

We mention the following researchers among them: Nedjma [6]used the golden section optimization approach to track the MPP during night[14] and in the face of fast meteorological changes. A modified PSO (MPSO) technique wasdeveloped by Sakthigokulrajan and Ravi[2]. The main benefit of modified particle swarm optimizationMPSO, according to the authors, is the reduction in steady-state oscillation once the MPP is attained Sakthigokulrajan and Ravi [2]. Soufyane, et al. [14] created the artificial bees colony (ABC) algorithm, which was experimentally confirmed in terms of resilience and efficiency [6]. The main contribution of this work is to provide artificial intelligence-based control approaches fortheglobal maximum power point tracking GMPPT to find the global maximum power point GMPPT. In the year 2020, Nedjma [6],created aproject about the design of an optimal MPPT control based on artificial intelligence [6]. We relied on the reason for the results obtained in making our controller model and applying it to our PV grid model[6, 11, 15].

The main contributions of this approach are:

- Design of IC, FL, VSIand PSO algorithm control technic for decreasing tracking error while tracking for the maximum power point are the primary contributions of this approach.
- The dynamic performance of these controllers: IC, FL, VSI and PSO are highlighted in this paper through a comparison, which controls the grid's active and reactive powers.

2. Grid-Connected Pv System Proposed In The Study

The PV system employed in this study is the 100kW PV system connected to the electrical grid that we used in our previous work, as shown in Figure10.Table1lists the primary parameters that define this PV system.

Table1. Parameters characterizing the proposed grid-connected PV system are listedin.

	PV module model	MPPT-305-WHT-U
PV parameters	PV array power	100.7 kW
	PV current	368.28 A
	PV voltage	273.5 V
	DC/DC chopper output voltage	500 V
Direct Current Voltage DC link	Capacity	0.012 F
	DC link voltage	500 V

parameters	Switching frequency	5 kHz
network settings	Voltage (Vrms)	25 kV
	Current (Vrms)	1.76 A
	frequency	50 Hz
load parameters	active power	30 kW
	Reactive power	10 kVAR
	frequency	50 Hz

The PV system described in this work is based on two models[6, 11] and it is primarily equipped with:

- A PV field with 66 parallel branches.

  Each branch is made out of 5 305 kW PV modules.

- An MPPT control, a boost converter, and a three-phase inverter with a control stage comprise the adaption step.

  This system has two stages of control, as shown in Figure 1:

- The maximum power point (MPP) controller is used in the DC/DC control stage, and the DC/AC control stage contains two control loops, which increases DC/AC control efficiency.
  This controller, as shown in Figure 2, increases the efficiency of DC/AC control

This three-phase inverter controller contains an internal DC coupling direct current Voltage control loop, as shown in Figure 2.aandFigure 2.b This voltage control allows the voltage to be regulated to its optimal value to supply current to the DC link. The phase-locked loop's forward and quadrature currents (Id, Iq) are controlled by the second loop, which is the outer loop. Each of these two loops is regulated by a PI controller, whose gains are altered using metaheuristic techniques to increase the grid-connected PV system's dynamic performance.

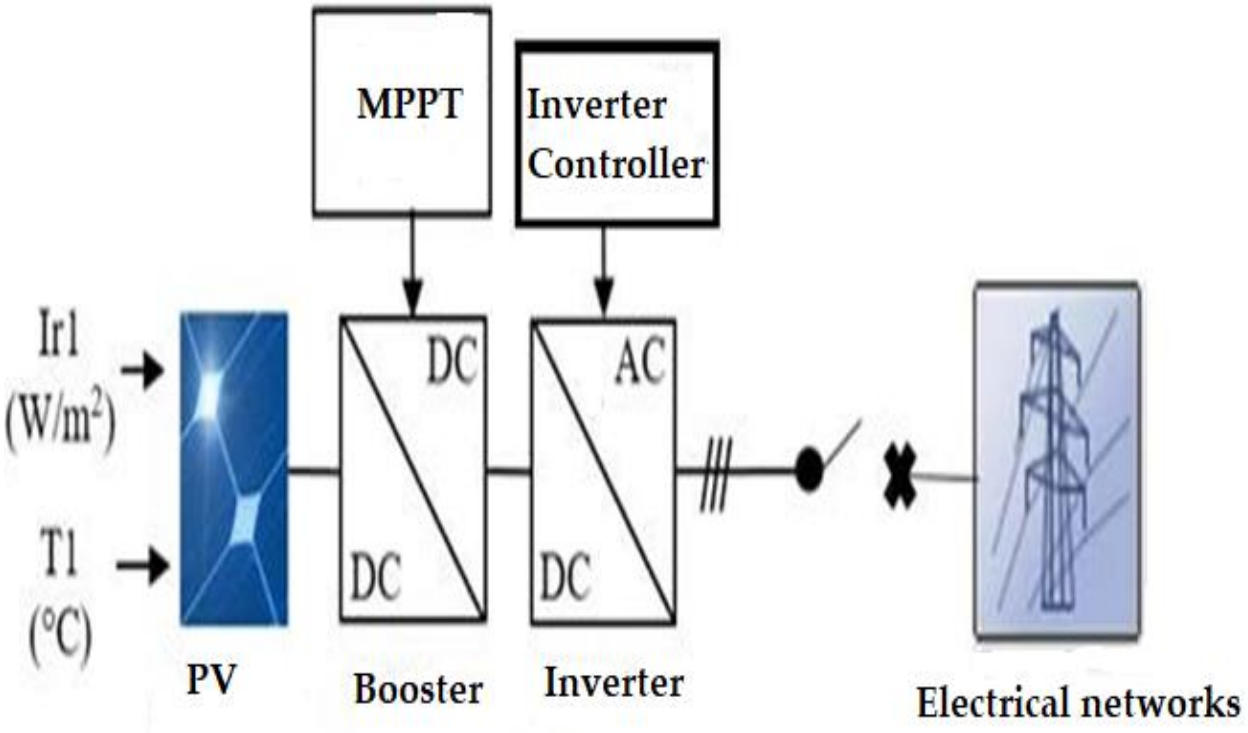

Figure 1. Photovoltaic system with a 100-kilowatt output that is connected to the grid[6].

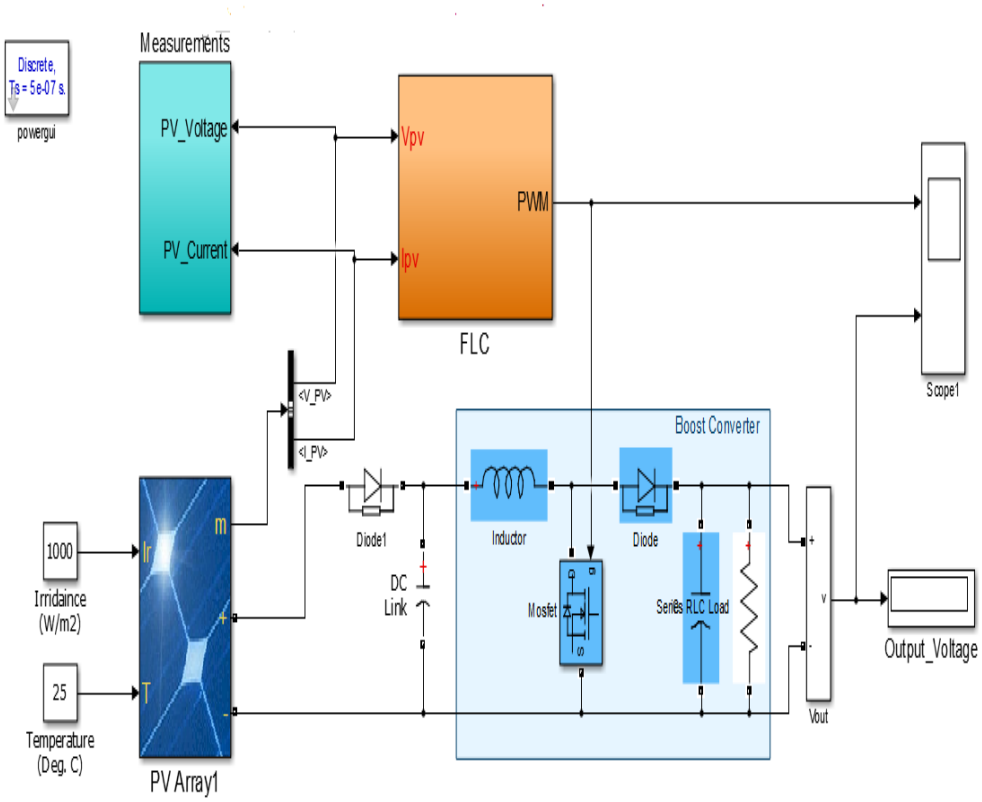

Figure 2.a. Control scheme for three-phase inverters [6, 11]

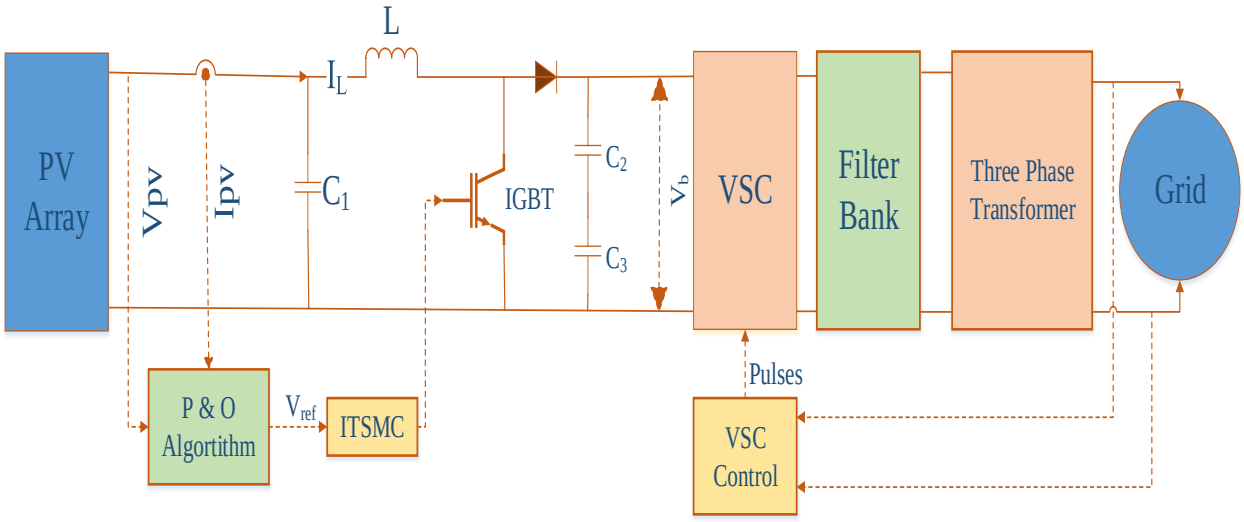

Figure 2.b. Control scheme for three-phase inverters[11]

3. Modelling A Pv Array's Characteristics

A PV grid converts solar energy into electricity using one or more PV arrays. A PV cell is the basic unit of a PV array, and it works on the photovoltaic principle. When the photon energy is greater than the band gap energy, the photovoltaic effect occurs, which is described as the conversion of light into electrical energy by outer electrons breaking the bond in a semiconductor device.Equation 1 presentsa semiconductor diode ofa PV cell with the Shockley diode equation[13] :

$$I_D = I_o\left[exp\left(\frac{qV_{PV}}{AKT}\right) - 1\right] \quad (1)$$

Equation 2 arguesthe PV cell's output current I_PV and Equation 3presentsa saturation current I_o are calculated as:

$$I_{PV} = I_{SC} - I_o\left[exp\left(\frac{qV_{PV}}{AKT}\right) - 1\right], \quad (2)$$

$$I_o = I_{or}\left[\frac{T}{T_R}\right]^3 \exp\left(\frac{qE_g}{K\alpha}\left[\frac{1}{T_R} - \frac{1}{T}\right]\right) \quad (3)$$

3.1. Modeling of Boost Converter and MPPT

Figure 3 depicts the I-V characteristics of a PV cell [11] highlighting the importance of short circuit current (highest current at zero load) and open circuit voltage (voltage at zero current). The maximum power point can be obtained by using the highest voltage V, MPP and current, as shown in the figure.

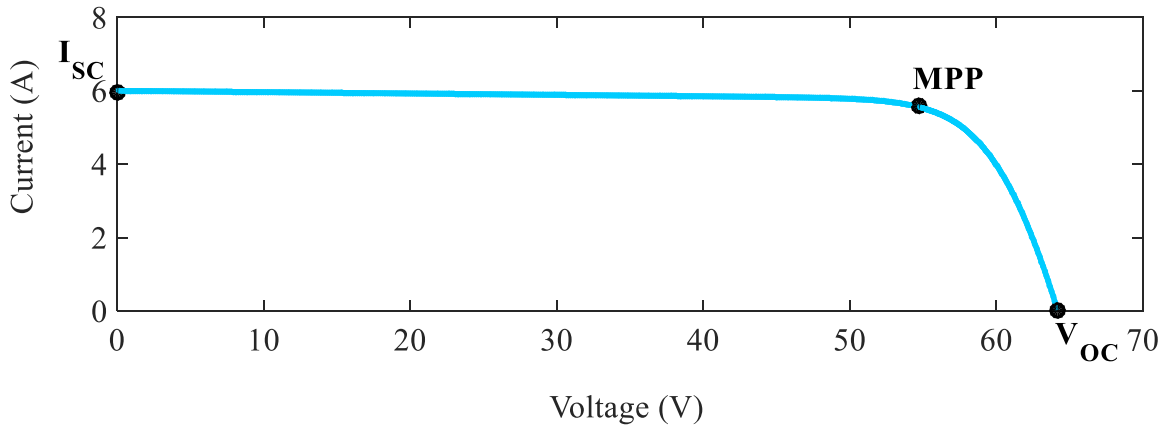

Figure 3. I-V characteristic curve of a PV array.

V_MPP tracking is required for maximum power extraction. MPPT algorithms can be used to improve the efficiency of a system employing MPP tracking [14]. MPPT methods include perturb and observe, incremental conductance, fractional circuits, and fuzzy networks [16]. The perturb and observe technique is used in this paper because of its ease of implementation and cost-effectiveness. By tracking the maximum power point, this technique generates a reference voltage.

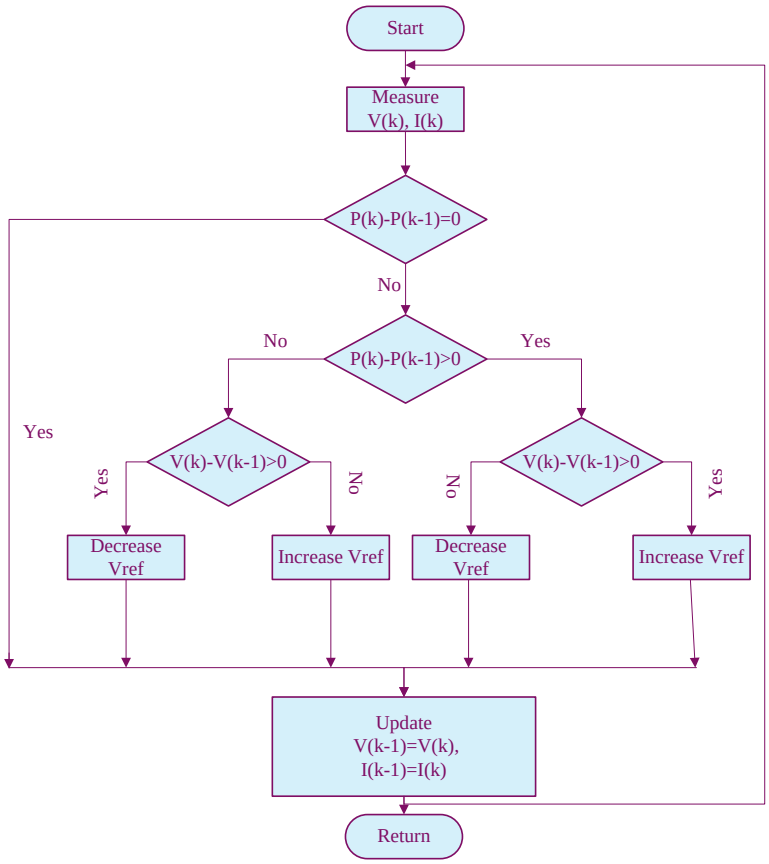

Figure 4. Flowchart for perturb and observe algorithm[11].

Figure 4depicts theperturb and observe algorithm, which demonstrates how the reference voltage V ref changes in response to the PV array's power output. When there is a power decrease, perturbation is usually in the same direction as the power increase, and when there is a power decrease, perturbation is in the other direction [17]. The process of observation and perturbation continues until the maximum power point is reached, and a reference voltage is found, which should be compared to the voltage generated V_PV. The difference between these two voltages must be regulated so that it does not change the duty cycle of the maximal power, which affects the boost converter's output voltage.

As a result, the duty cycle of pulse widthmodulationPWMdelivered to IGBT can be controlled. In a boost converter, the error between the generated and reference voltage must be regulated.

A DC-DC boost converter's current at the capacitor C_1 with an inductor current I_L is defined as:

$$I_{C_1} = C_1 \frac{dV_{PV}}{dt} = I_{PV} - I_L \quad (4)$$

With u as the duty cycle and V_b as the bulk voltage across the capacitor C_2, the voltage across the inductor L is given by:

$$V_L = L \frac{dI_L}{dt} = V_{PV} - V_b(1-u) \quad (5)$$

3.2. Voltage Source Inverter

In this paper, a current-controlled three-phase voltage inverter is employed. The boost converter provides a steady DC voltage to the VSI. A three-phase inverter's output voltage is generated by driving the gates and switches. If the inductor currents and capacitor voltage are treated as state variables, the state-space representation [11, 18] of a three-phase VSI coupled to a grid is as follows:

$$\dot{I}_a = -\frac{R_1}{L_1} I_a - \frac{1}{L_1} V_{a\_mes} + \frac{V_{PV}}{3L_1}(2s_a - s_b - s_c) \quad (6)$$

$$\dot{I}_b = -\frac{R_1}{L_1} I_b - \frac{1}{L_1} V_{b\_mes} + \frac{V_{PV}}{3L_1}(-s_a + 2s_b - s_c) \quad (7)$$

$$\dot{I}_c = -\frac{R_1}{L_1} I_c - \frac{1}{L_1} V_{c\_mes} + \frac{V_{PV}}{3L_1}(-s_a - s_b + 2s_c) \quad (8)$$

$$\dot{V}_{PV} = \frac{1}{C} I_{PV} - \frac{1}{C}(I_a s_a + I_b s_b + I_c s_c) \quad (9)$$

Each phase of VSI is represented by the switching signals s_a,s_b, and $s_c$care. The grid and inverter output filter's total inductance is L_1, with an equivalent series resistance of R_1.

To regulate the gates, VSI requires pulses, which are generated by PWM. VSI control generates these pulses, and the VSI control block diagram is given in Figure5. PWM takes the three modulating signals U_{abc_Ref} as input. The output voltages V_d and V_q of a current controller generate these three modulating signals. Thus, for a simpler control design, transformations for the state space model must be implemented, which can be done via park or transformation.

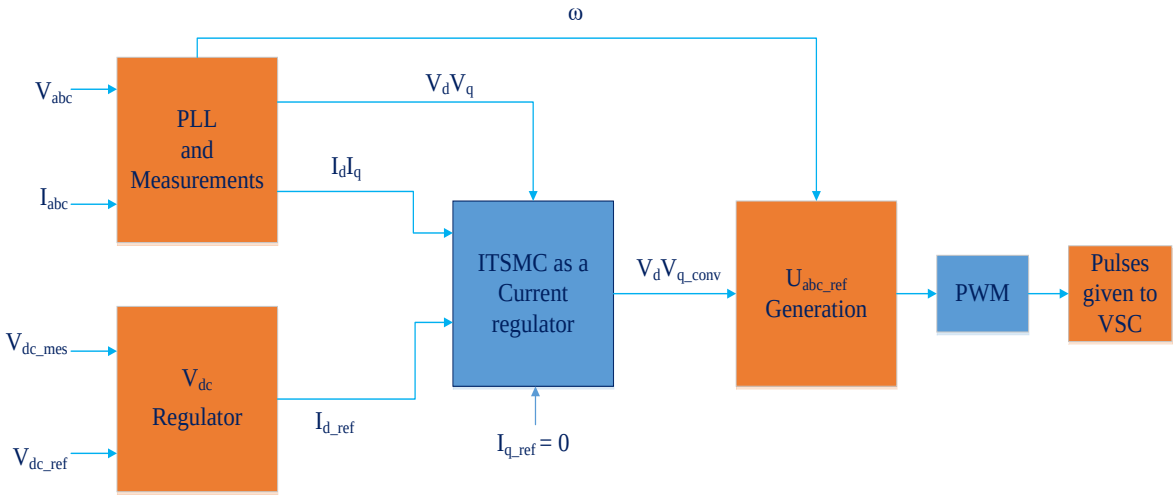

Figure 5. VSI control[11].

For VSI state space equations [11] applying dq transformation in synchronous frame can change them as illustrated below in the Figure 5.

$$\dot{I}_d = -\frac{R_1}{L_1} I_d + \omega I_q - \frac{1}{L_1} V_{d\_mes} + V_{d\_conv} \quad (10)$$

$$\dot{I}_q = -\frac{R}{L_1} I_q - \omega I_d - \frac{1}{L_1} V_{q\_mes} + V_{q\_conv} \quad (11)$$

$$\dot{V}_{PV} = \frac{1}{C} I_{PV} - \frac{1}{C} I_d s_d - \frac{1}{C} I_q s_q \quad (12)$$

Where V_{d_mes}andV_{q_mes}, $I_d$and I_q are the direct quadrature components of grid voltage and output current of the inverter, and I and I q are the direct quadrature components of grid voltage

and output current of the inverter, respectively. I_{d_ref}andI_{q_ref} are maintained zeros that are later used as one of the inputs in the current controller using the external DC link voltage regulator.

4. Control Scheme

In real-time applications, grid-connected PV systems are a type of nonlinear system with parameters perturbation, uncertainty and external disturbances. The IC, FC and PSO controllers provide a superior technical solution for non-affine nonlinear systems of this type by retaining the system error on an integral terminal sliding surface and then sliding the surface to zero. This paper discusses The IC, FC and PSO design for MPPT control [6].

4.1. MPPT Control

Consider the following switching variable β as a constant for MPPT control [11].

$$s = e(t) + \beta e_i(t) \tag{13}$$

Where: $e(t) = V_{pv} - V_{ref}$, $\ddot{e}(t) = sign(e(t))$.

Then there's the manifold that slides dσ is given as:

$$\sigma = \dot{e}(t) + \beta \dot{e}_i(t) \tag{14}$$

When $\dot{\sigma} = 0$, it is possible to obtain the control signal thus:

$$\dot{\sigma} = \ddot{e}(t) + \beta \ddot{e}_i(t) = 0 \tag{15}$$

$$\ddot{V}_{pv} - \ddot{V}_{ref} + \beta \ddot{e}_i(t) = 0 \tag{16}$$

We may get the expression of $\ddot{V}_{pv}$, which is substituted in (16)

$$\frac{1}{C_1}\left[\dot{I}_{pv} - \dot{I}_L\right] - \ddot{V}_{ref} + \beta \ddot{e}_i(t) = 0 \tag{17}$$

The control signal can be obtained by replacing (5) in (17) with a positive constant k.

$$u = \frac{1}{V_b}\left[L\dot{I}_{pv} + LC_1\beta\ddot{e}_i(t) - LC_1\ddot{V}_{ref} - V_{pv} + V_b - ksign(s)\right] \tag{18}$$

4.2. Clear Evidence

We know from the Lyapunov function that:

$$V = \frac{1}{2}\sigma^2 = 0 \quad (19)$$

V's derivative must be negative for it to guaranteeconvergence.

$$\dot{V} = \sigma\dot{\sigma} < 0 \quad (20)$$

When we replace Equation 15 with Equation 20, we get[11]:

$$\dot{V} = \sigma\{\ddot{e}(t) + \beta\ddot{e}_i(t)\} \quad (21)$$

$$\dot{V} = \sigma\left\{\frac{1}{C_1}[I_{PV} - I_L] - \dot{V}_{ref} + \beta\ddot{e}_i(t)\right\}$$

$$= \sigma\left\{\frac{1}{C_1}I_{PV} - \frac{1}{LC_1}V_{PV} + \frac{1}{LC_1}V_b(1-u) - \dot{V}_{ref} + \beta\ddot{e}_i(t)\right\}$$

$$= ||\sigma||\left\{||\frac{I_{PV}}{C_1}|| - ||\frac{V_{PV}}{LC_1}|| + ||\frac{V_b}{LC_1}|| - ||\frac{V_b}{LC_1}||u - ||\dot{V}_{ref}|| + \beta||\ddot{e}_i(t)||\right\} \quad (22)$$

When the control signal u is substituted in the preceding equation, the result is:

$$\dot{V} \le ||\sigma||\left\{-||\frac{V_b}{LC_1}||k\right\}$$

$$\dot{V} \le -||\sigma||\left\{||\frac{V_b}{LC_1}||k\right\} \quad (23)$$

The proof is completed by holdingEquation 23 in place, which ensures the exponential convergence of $e(t)$ to
" 0 ".

4.3. Control Scheme for VSI[11]

We get (10) and (11) when we rewrite the equations[11]:

$$V_{d\_mes} + I_d R_1 - I_q L_1 + \dot{I}_d L_1 = V_{d\_conv} \quad (24)$$

$$V_{q\_mes} + I_d L_1 + I_q R_1 + \dot{I}_q L_1 = V_{q\_conv} \quad (25)$$

Consider the sliding surfaces $s_d$and s_q, which are denoted by the letters s_d and s_q, respectively:

$$s_d = e_d + \alpha_d e_{i_d} \quad (26)$$

$$s_q = e_q + \alpha_q e_{i_q} \quad (27)$$

Where: $e_d = I_d - I_{d\_ref}, e_{i_d}^{\cdot} = sign(e_d)$ and $e_q = I_q - I_{q\_ref}$, $e_{i_q}^{\cdot} = sign(e_q)$. Control signals are obtained when $\dot{s}_d = 0$ and $\dot{s}_q = 0$. When $\dot{s}_d = 0$ then,

$$\dot{e_d} + \alpha_d e_{i_d}^{\cdot} = 0$$

$$\dot{I_d} - \dot{I}_{d\_ref} + \alpha_d e_{i_d}^{\cdot} = 0 \qquad (28)$$

Equations 24and 28are combined to produce:

$$\frac{V_{d\_conv}}{L_1} + I_q\omega - \frac{I_d R_1}{L_1} - \frac{V_{d\_mes}}{L_1} = \dot{I}_{d\_ref} - \alpha_d e_{i_d}^{\cdot}$$

$$V_{d\_conv} = L_1\dot{I}_{d\_ref} - L_1\alpha_d e_{i_d}^{\cdot} - L_1 I_q\omega + I_d R_1 + V_{d\_mes} - k_d sign(s_d) \qquad (29)$$

Therefore,

$$V_{q\_conv} = L_1\dot{I}_{q\_ref} - L_1\alpha_q e_{i_q}^{\cdot} + L_1 I_d\omega + I_q R_1 + V_{q\_mes} - k_q sign(s_q) \qquad (30)$$

Clear evidence:
According to the Lyapunov function,

$$V = \frac{1}{2}s^2 = 0 \qquad (31)$$

When the gradient of V only is negative, V is given by the following formula to converge.

$$\dot{V} = s\dot{s} < 0 \qquad (32)$$

Assume $\dot{V}_d$ and afterwards replace Equation 27 with it to get:

$$\dot{V}_d = s_d\{\dot{e_d} + \alpha_d e_{i_d}^{\cdot}\} \qquad (33)$$

We may simplify the preceding equation as follows using Equations 24and 28:

$$\dot{V}_d = \frac{s_d}{L_1}\left\{V_{d\_conv} + I_q\omega L_1 - I_d R_1 - V_{d_{mes}} - \dot{I}_{d_{ref}} L_1 + \alpha_d e_{i_d}^{\cdot} L_1\right\} \qquad (34)$$

WhenEquation 29is substituted in the above equation, the result is:

$$\dot{V}_d = \frac{s_d}{L_1}\left\{L_1\dot{I}_{d\_ref} - L_1\alpha_d e_{i_d}^{\cdot} - L_1 I_q\omega + I_d R_1 + V_{d\_mes} - k_d sign(s_d) + I_q\omega L_1 - I_d R_1 - V_{d_{mes}} - \dot{I}_{d_{ref}} L_1 + L_1\alpha_d e_{i_d}^{\cdot}\right\}$$

$$\Rightarrow \dot{V}_d = \frac{s_d}{L_1}\{-k_d sign(s_d)\} \qquad (35)$$

$$\dot{V}_d < -\left\|\frac{s_d}{L_1}\right\| \{k_d sign(s_d)\} \quad (36)$$

Equally,

$$\dot{V}_q < -\left\|\frac{s_q}{L_1}\right\| \{k_q sign(s_q)\} \quad (37)$$

As a result, it is stable.

4.4. Fuzzy Control Algorithm[6]

FL is a novel artificial intelligence-based method. The FL [6] as shown in Figure 6, outperforms the standard IC algorithm in terms of robustness, stability, and ease of implementation[6, 19, 20]. The FL controller's primary goal, like that of other MPPT controllers, is to reach the MPP. The execution of this directive, however, is largely dependent on human skill [6]. The FL method is based on the decomposition of a real variable's range of variation into linguistic variables and assigning a membership function to each variable [1, 3, 4, 11, 16, 20-29]. The rules derived from the human operator's competence are conveyed in language form. The dynamic performance of the FL controller is determined by these rules. The proposed FL controller has four basic components: a fuzzification unit, base rules, inference motor, and defuzzification[16, 21-23]. The conversion of real variables to phantom variables is the focus of the fuzzification unit. E(k) and CE(k) are control entries for the FL provided by the Equations 38 and 39. E(k) stands for the P_{PV} derivation (k). When the point of operation reaches the MPP, E(k) is terminated. CE(k) is an error made by E. (k). The tension and current are measuredto calculate the P_{PV} power. The output of the FL dD controller is the only variable in the cyclic relationship[6, 11].

$$E(K) = \frac{I(K)-I(K-1)}{V(K)-V(K-1)} + \frac{I(K)}{V(K)} \quad (38)$$

$$CE(K) = E(K) - E(K-1) \quad (39)$$

The symmetric triangular form is considered the most suited among the several forms of membership functions (trapezium, Gaussian, and triangular, etc.) Figure 6. The range of fuzzy variables is often adjusted between 1 and +1 by using a gain factor to represent the genuine signals [30-33]. The symmetric triangle form was used for this investigation, and the boundaries were set at 935 ([-0.04, 0.04], [-100, 100], and [-0.04, 0.04], respectively, for (E, CE, and dDWhich represent the error between the inputs and the outputs where dDis theoutput barycenter calculated by defuzzification.

- Mamdani'sapproach[1, 4, 6, 11, 15, 24-32, 34-36] is used to accomplish fuzzy inference. (BP: large positive (big positive)), (SP: small positive), (ZE: zero), (SN: slightly negative (small negative)), and (BN: huge negative (big negative)) are the variables [1, 3, 4 and28]. The applied rules ensure that the relationship between the FL controller's inputs and outputs are listed in Table 2. For constant growth systems, the symmetric rule basis is commonly utilized [1, 3, 4, 11, 15, 25-32, 34-37].
- Defuzzification calculates the output dD, which is the barycenter, using the centroid method [1, 3, 4, 11, 15, 27-31, 34].

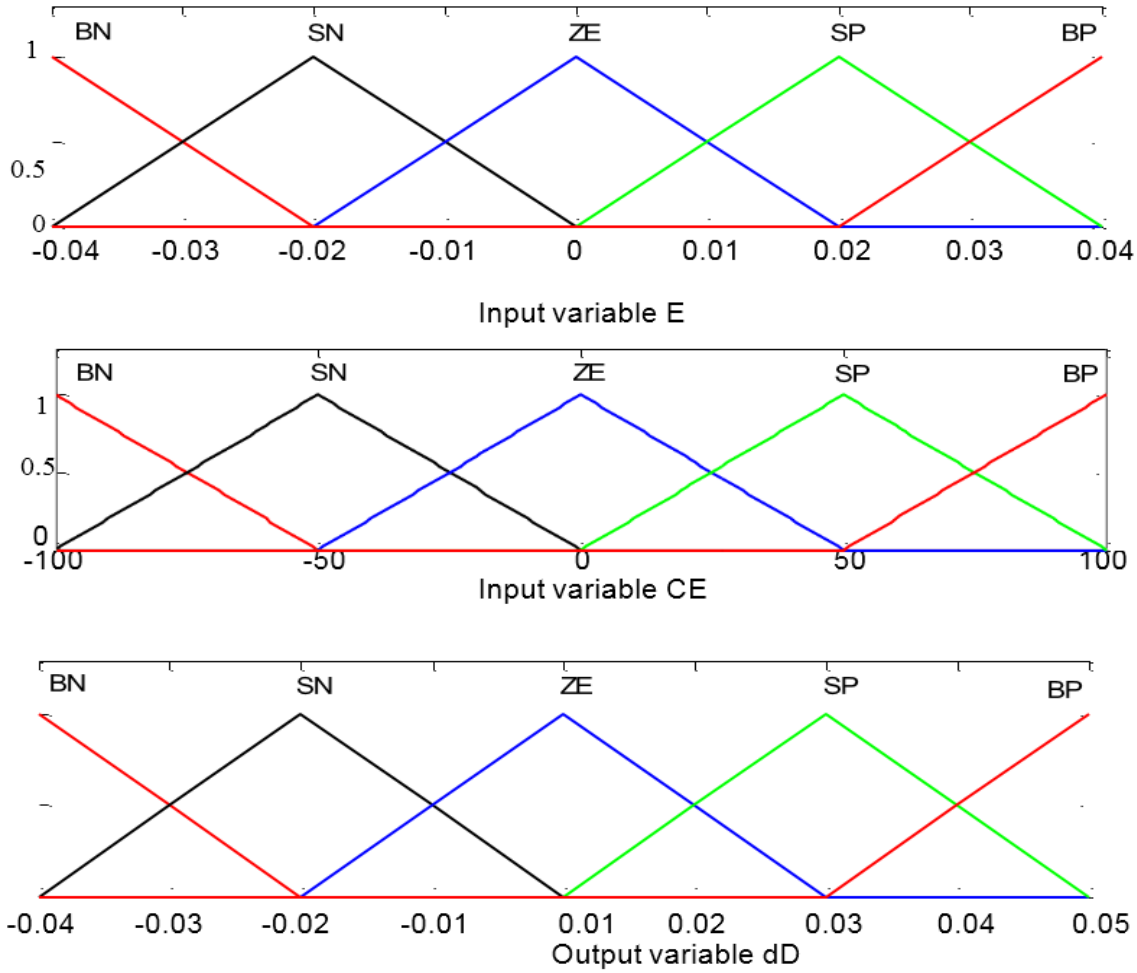

Figure 6. Input CE, ET and output (dD) variable membership functions[6].

Table 2. FL fuzzy logic rules[6].

CE / E	BN	SN	ZE	SP	BP
BN	ZE	ZE	BP	BP	BP

SN	ZE	ZE	SP	SP	SP
ZE	SP	ZE	ZE	ZE	SN
SP	SN	SN	SN	ZE	ZE
BP	BN	BN	BN	ZE	ZE

Where: (BP: large positive (big positive)), (SP: small positive), (ZE: zero), (SN: slightly negative (small negative)), and (BN: huge negative (big negative)) are the inputs variables, Nedjma [6].

4.5. Particle Swarm of Optimization Algorithm

PSO is a metaheuristic global search approach based on same-group particles' common and self-organizing activity [6,11, 32 and34]. As shown in Figure 7, displacement rules (in the space of solutions) regulate this strategy, which allows these particles to progressively shift from their random places to an ideal local position [36, 37].

The parameters of the PSO are listed in Table 3, and the particle's position is corrected based on its updated speed (velocity), best personal position achieved (PBest), and best position obtained in the region (GBest). The PSO is based on the Equations 38 and 39[1, 4, 11, 16, 21-27, 33] which describe how to update the local and global positions of particles and the group:

$$V_i(t+1) = w * \left[V_i(t) + c_1 * rand_1 * \left(PBest_i(t) - D_{fitness_i}(t)\right) + c_2 * rand_2 * (GBest_i(t) - P_i(t))\right] \quad (40)$$

$$P_i(t+1) = P_i(t) + V_i(t+1) \quad (41)$$

$$D = PSO(V, I) \quad (41)$$

Where:

- P: is the particle's position;
- V stands for velocity; and
- PBest is the particle's best position, which corresponds to Local Dbest.

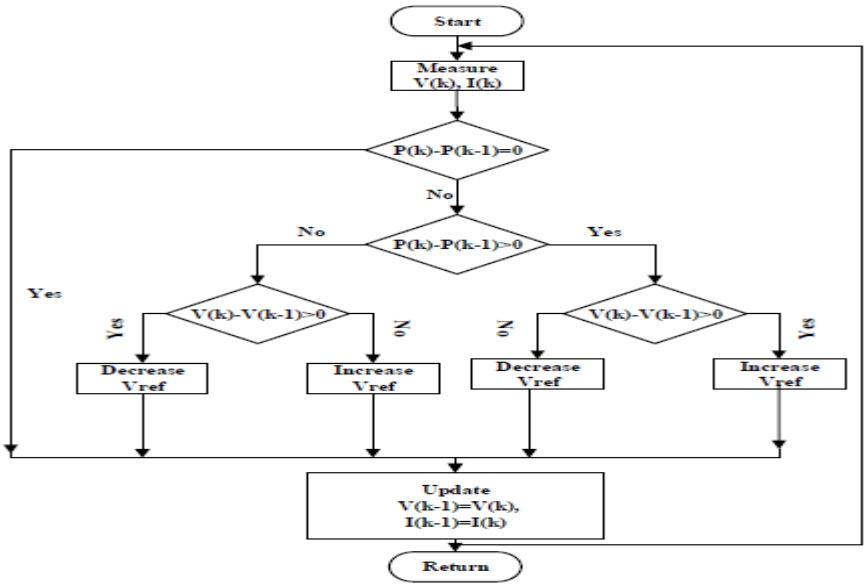

Figure 7. The PSO's organizational chart [6].

- GBest: The particle group's best position, which corresponds to Global Dbest;

Rand: A random variable with a uniform distribution over the range [0, 1] (function defined in MATLAB); and D stands for duty cycle.

Table 3. PSO algorithm parameter[6].

Parameters	**Symbole**	**Valeur**
Number of swarms	Swarms	10
Number of iterations	iter_max	20
Weight of local information	c1	0.02
Weight of global information	c2	0.05
Weight of inertia	w	0.5
Dimension of the problem	Dim	1
Global maximum power point	GMPP	0

The PSO flowchart [6]shown in Figure 7is dependent on satisfying Equation42. The steps in this flowchart are as follow: Table 3 shows the initialization of the PSO parameters. Particles, locations, and velocity are all initialized. The initialization of the particles entails setting the old and new components of the photovoltaic power vectors to zero:

PPV Old = 0 (1, swarming).

PPV New = 0 (1, swarms)

4.6. Conductance Increment (CI) Algorithm

The conductance increment (IC) algorithm is a traditional MPPT method that employs two probes to monitor the PVmodule's operational voltage V and current I. This method is based on the fact that at the maximum power point (MPP), the derivative of the output power P with respect to the voltage V of the PV module is equal to zero [6, 11]. As a result, we have the following equations: [6, 21].

$$\frac{dP}{dV} = \frac{d(VI)}{dV} = I\frac{dV}{dV} + V\frac{dI}{dV} = I + V\frac{dI}{dV} \quad (42)$$

$$\frac{dP}{dt} = 0 \Leftrightarrow \frac{dI}{dV} = -\frac{I}{V} \quad (43)$$

To reach the MPP, the primary function in the CI algorithm shown in Figure 8 requires the following conditions:

$$\frac{dI}{dV} = -\frac{I}{V} \quad For\ V = V_{mp} \quad (44)$$

$$\frac{dI}{dV} > -\frac{I}{V} \quad For\ V < V_{mp} \quad (45)$$

$$\frac{dI}{dV} < -\frac{I}{V} \quad For\ V > V_{mp} \quad (46)$$

The voltage that corresponds to the MPP is calledV_{mp}. If Equation 43 holds, the PV system has reached the MPP and no adjustment in the operating voltage is required; otherwise, the operating voltage is adjusted as needed.

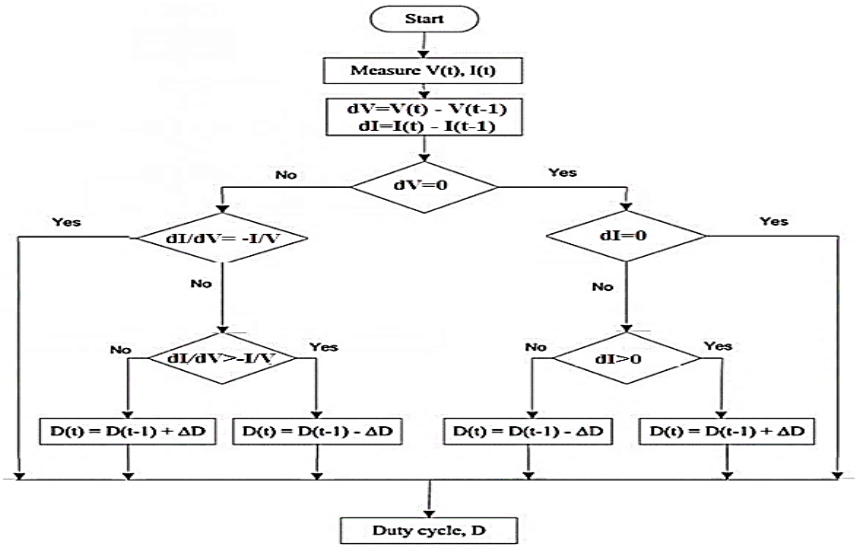

Figure 8. Flowchart of the incremental conductance algorithm[6].

5. Simulation Results

The goal of this essay wasto create an AI-based MPPT control that can cope with various atmospheric fluctuations.

Given the effects of lighting and temperature, this research examined the MPPT methods chosen (IC, FL, and PSO) and assessed their dynamic behavior in terms of stability, speed, and efficiency.

The simulation wasrun for 1000W/m2 uniform and constant illumination conditions with a temperature of 25°C. The synoptic diagram and model provided for the simulation of the PV system of 100 kW connected to the distribution network under Matlab/Simulink are shown in Figures 9.

A 100 kW 1000 W/m2 PV generator is connected to a 25 kV grid using a boost DC/DC chopper and a three-phase three-level voltage inverter in this setup. In the boost converter, the MPPT controller is implemented. In this case, We chose the boost type converter since the PV generator can give a maximum voltage of 273.5 volts and a current of 368.28 ampere at the input of the DC-DC converter, and we required 500 volts at the input of the three-phase inverter. The PV generator is made up of 66 PV strings that are joined in series. Each PV string is made up of five PV modules that are linked in series. Each PV module is made up of 96 PV cells that are linked in series.

Table 4 lists the model parameters for the PV modules that were used.

Table 4. PV Generator specifications.

Results	PV Module Features						
	Model	Number OfCells	Vm(V)	Im(A)	MPP (kW)	ISC(A)	VOC(V)
PV module features	Sun Power SPR-305WHT	96	54.7	5.58	0.305	5.96	64.2
Features of 100 kW PV Generator			273.5	366.39	100.208	35.87	57.8

Where : 1- VOCis an open circuit voltage.

2- ISC indicates the short circuit current.

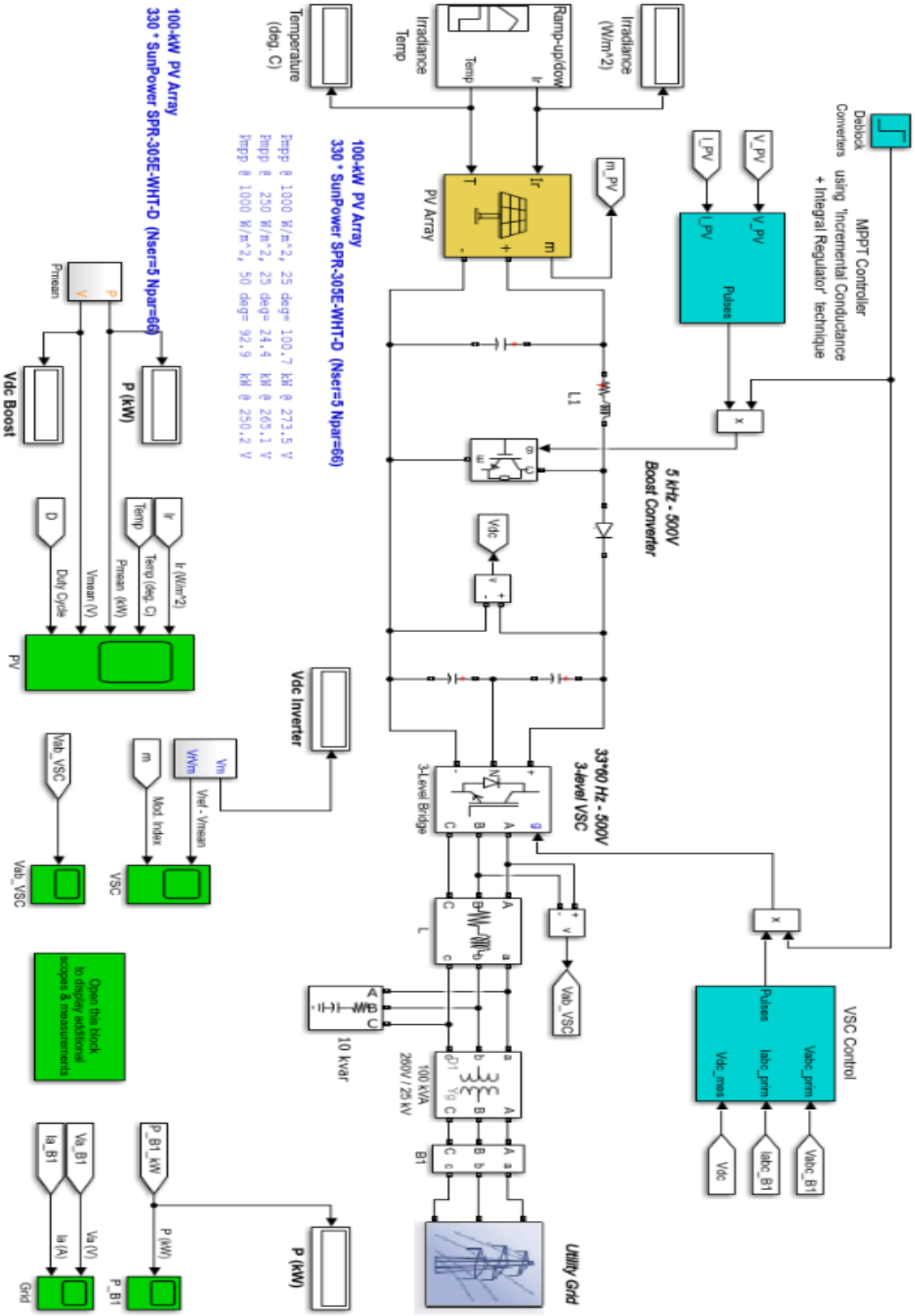

Figure 9. Grid connected PV model[11].

The dynamic performance of PV power, PV voltage, duty cycle, and grid-level power is shown in Figure 9. To begin, the suggested PV system was simulated under homogeneous light, which corresponded to normal circumstances of 1000 W/m2 and 25 degrees Celsius. According to Figure 9 and Table 4, the IC approach had the poorest statistical parameters, and its dynamic behavior was marked by substantial ripples, which hada detrimental impact on PV system operation. The FL had the quickest response time and accurately tracked illumination variations. The PSO approach had a 99.35 percent effectiveness rate. Figure 10indicates that the simulation results suggest that the PSO is superior to the others. Simulations show that the algorithms FL, VSI and PSO can track changes in illumination and temperature to achieve the MPP.Figure 11illustratesdynamic response of PSO algorithm control in grid-connected PV System and shows that PSO outperforms them especially during the night and/or in partial shaded areas during the day. Undesirable ripples in Figure 12andFigure 13 appear in the IC's and VSI's dynamic reaction, which is a dangerous disadvantage for the PV system.

The PV power produced using PSO was clearly superior to that obtained with FL, VSI and IC approaches especially during partial shade.

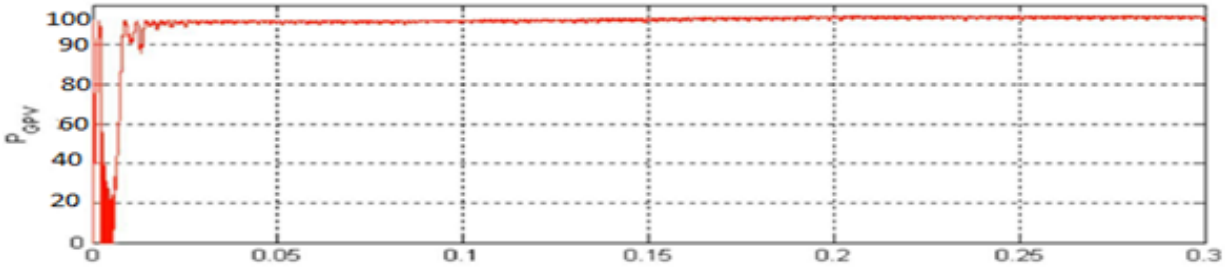

Figure 10. Dynamic response of the 100 kW grid-connected PV System with FLC control.

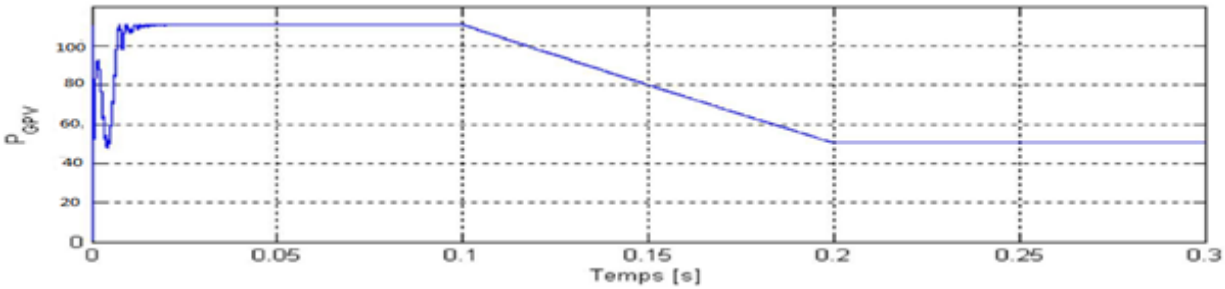

Figure 11. Dynamic response of the 100 kW grid-connected PV System with PSO control.

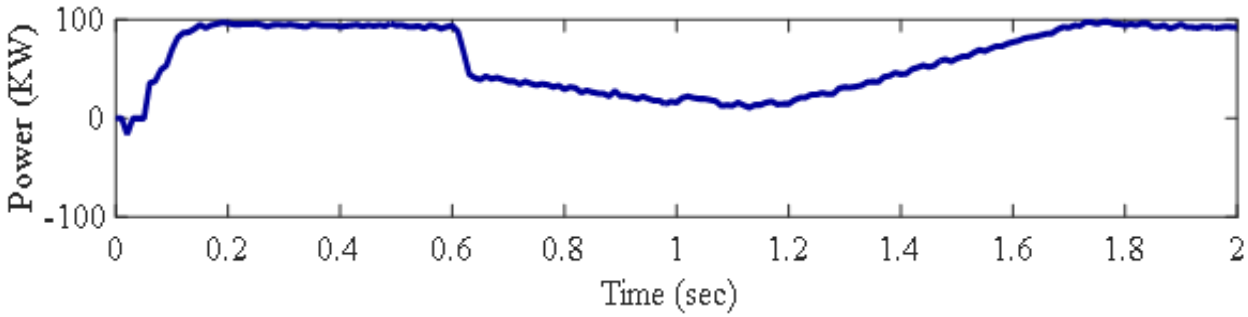

Figure 12. Dynamic response of the 100 kW grid-connected PV System with IC control.

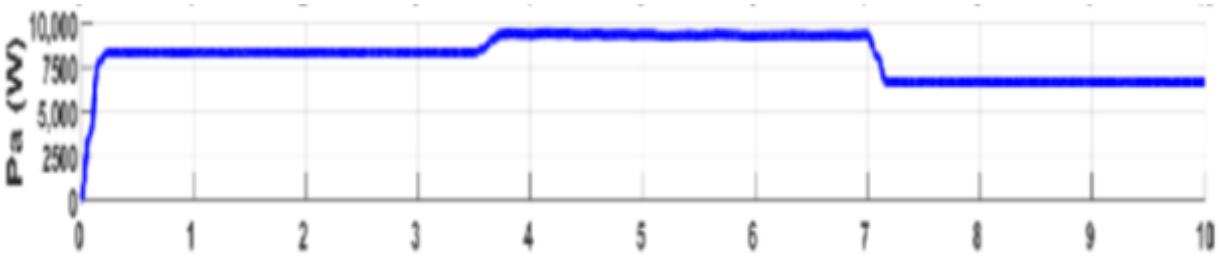

Figure 13. Dynamic response of the 100 kW grid-connected PV System with VSI control.

6. Conclusion

This article provides an overview of some of the most widely used MPPT approaches cited in the literature. We chose three types of MPPT methods in this study: the classical method (IC), the artificial intelligence-based method (FL), and the metheuristic approach (PSO). The chosen model was described in detail. This model is a 100 kW PV system with a distribution network connection. Under various atmospheric conditions, we compared the IC, FL, VSI and PSO approaches in terms of efficiency, speed, and robustness. When compared to other proposed strategies such as VSI, IC and FL, simulation findings showed that PSO outperformed them especially during partial shade.

Nomenclature

PV	Photovoltaic.
P & O	Perturb and observe.
MPPT	Maximum power point tracking.
MPP	Maximum power point.
VSI	Voltage source inverter.
SMC	Sliding mode control.
IGBT	Insulated gate bipolar transistors.
Current generated by incident light (or) Short circuit current.	
V_{OC}	Open circuit voltage.
I_o	Reverse saturation current.

q Electron charge $=1{,}602\,10^{-19}$coulomb

K Boltzmann constant $=1{,}38 * 10^{-23}\frac{J}{K}$

T Temperature of p-n junction in kelvin.
A Ideal diode constant.
I_{or} Nominal saturation current.
T_R Nominal temperature.
E_g Band gap energy of the semiconductor.

Funding: This study received no specific financial support.
Competing Interests: The authors declare that they have no competing interests.
Acknowledgement: Both authors contributed equally to the conception and design of the study.

References

[1] J. Mohammad and AfefFekih, "Integral terminal sliding mode control to provide fault ride-through capability to a grid connected wind turbine driven DFIG," presented at the IEEE International Conference on Industrial Technology (ICIT), 2015.

[2] C. Sakthigokulrajan and K. Ravi, "RETRACTED: Combined role of derived array configurations and MPSO based MPPT in improving the energy yield under partial shading conditions. ," *Journal of Building Engineering,* vol. 9, pp. 125-134, 2017.Available at: https://doi.org/10.1016/j.jobe.2016.12.006.

[3] S. A. Fayaz, Z. Majid, and A. B. Muheet, "Knowledge discovery in geographical sciences—A systematic survey of various machine learning algorithms for rainfall prediction," presented at the International Conference on Innovative Computing andCommunications. Springer, Singapore, 2022.

[4] T. Esram and P. L. Chapman, "Comparison of photovoltaic array maximum power point tracking techniques," *IEEE Transactions on Energy Conversion,* vol. 22, pp. 439-449, 2007.Available at: https://doi.org/10.1109/tec.2006.874230.

[5] N. Shah and C. Rajagopalan, "Experimental evaluation of a partially shaded photovoltaic system with a fuzzy logic-based peak power tracking control strategy," *IET Renewable Power Generation,* vol. 10, pp. 98-107, 2016.Available at: https://doi.org/10.1049/iet-rpg.2015.0098.

[6] A. Nedjma, "Nedjma aouchiche. Design of an optimal MPPT control based on artificial intelligence of a photovoltaic system. Other. Bourgogne Franche-Comté University," 2020.

[7] Y. Tan, L. Meegahapola, and K. M. Muttaqi, "Suboptimal MPPT control for power management in PV-diesel remote area power supply systems," presented at the 2014 IEEE Industry Application Society Annual Meeting. IEEE, 2014.

[8] A. Tabanjat, M. Becherif, M. Emziane, D. Hissel, H. Ramadan, and B. Mahmah, "Fuzzy logic-based water heating control methodology for the efficiency enhancement of hybrid PV–PEM electrolyser systems," *international Journal of Hydrogen Energy,* vol. 40, pp. 2149-2161, 2015.Available at: https://doi.org/10.1016/j.ijhydene.2014.11.135.

[9] K. Ş. Parlak, "PV array reconfiguration method under partial shading conditions," *International Journal of Electrical Power & Energy Systems,* vol. 63, pp. 713-721, 2014.Available at: https://doi.org/10.1016/j.ijepes.2014.06.042.

[10] S. Lyden and M. Haque, "Maximum power point tracking techniques for photovoltaic systems: A comprehensive review and comparative analysis," *Renewable and Sustainable Energy Reviews,* vol. 52, pp. 1504-1518, 2015.Available at: https://doi.org/10.1016/j.rser.2015.07.172.

[11] S. T. A. Sai, J. M. Mohammad, and F. Afef, "Integral terminal sliding mode control for maximum power production in grid connected PV systems," presented at the IEEE Conference on ControlvApplications (CCA) Part of 2016 IEEE Multi- Conference on Systems and Control September 19-22, 2016. Buenos Aires, Argentina, 2016.

[12] S. Choudhury and P. K. Rout, "Comparative study of M-FIS FLC and modified P&O MPPT techniques under partial shading and variable load conditions," presented at the 2015 Annual IEEE India Conference (INDICON). IEEE, 2015.

[13] F. Belhachat and C. Larbes, "Global maximum power point tracking based on ANFIS approach for PV array configurations under partial shading conditions," *Renewable and Sustainable Energy Reviews,* vol. 77, pp. 875-889, 2017.Available at: https://doi.org/10.1016/j.rser.2017.02.056.

[14] B. A. Soufyane, A. Chouder, K. Kara, and S. Silvestre, "Artificial bee colony based algorithm for maximum power point tracking (MPPT) for PV systems operating under partial shaded conditions," *Applied Soft Computing,* vol. 32, pp. 38-48, 2015.Available at: https://doi.org/10.1016/j.asoc.2015.03.047.

[15] S. S. T. Amirineni, *Integral terminal sliding mode control design for grid-connected photovoltaic systems* University of Louisiana at Lafayette, 2017.

[16] E. Bianconi, J. Calvente, R. Giral, E. Mamarelis, G. Petrone, C. A. Ramos-Paja, G. Spagnuolo, and M. Vitelli, "Perturb and observe MPPT algorithm with a current controller based on the sliding mode," *International Journal of Electrical Power & Energy Systems,* vol. 44, pp. 346-356, 2013.Available at: https://doi.org/10.1016/j.ijepes.2012.07.046.

[17] T. Zhou and W. Sun, "Study on maximum power point tracking of photovoltaic array in irregular shadow," *International Journal of Electrical Power & Energy Systems,* vol. 66, pp. 227-234, 2015.Available at: https://doi.org/10.1016/j.ijepes.2014.10.030.

[18] J. Samimi, E. A. Soleimani, and M. Zabihi, "Optimal sizing of photovoltaic systems in varied climates," *Solar Energy,* vol. 60, pp. 97-107, 1997.Available at: https://doi.org/10.1016/s0038-092x(96)00165-x.

[19] Z. Majid, K. Sameer, and A. Muheet, "Analytical comparison between the information gain and gini index using historical geographical data," *International Journal of Advanced Computer Science and Applications,* vol. 11, pp. 429-440, 2020.

[20] D. G. Montoya, C. A. Ramos-Paja, and R. Giral, "Improved design of sliding-mode controllers based on the requirements of MPPT techniques," *IEEE Transactions on Power Electronics,* vol. 31, pp. 235-247, 2015.Available at: https://doi.org/10.1109/tpel.2015.2397831.

[21] H. M. Hasanien, "An adaptive control strategy for low voltage ride through capability enhancement of grid-connected photovoltaic power plants," *IEEE Transactions on Power Systems,* vol. 31, pp. 3230-3237, 2015.Available at: https://doi.org/10.1109/tpwrs.2015.2466618.

[22] C.-S. Chiu, "Derivative and integral terminal sliding mode control for a class of MIMO nonlinear systems," *Automatica,* vol. 48, pp. 316-326, 2012.Available at: https://doi.org/10.1016/j.automatica.2011.08.055.

[23] X. X. Liu and L. A. C. Lopez, "An improved perturbation and observation maximum power point tracking algorithm for PV arrays," in *Proceedings of IEEE Power Electronics Specialist Conference*, 2004.

[24] H. S. Rauschenbach, *Solar cell array design handbook.* New York: Van Nostrand Reinhold, 1980.

[25] S. Dhar and P. Dash, "Adaptive backstepping sliding mode control of a grid interactive PV-VSC system with LCL filter," *Sustainable Energy, Grids and Networks,* vol. 6, pp. 109-124, 2016.Available at: https://doi.org/10.1016/j.segan.2016.03.001.

[26] M. A. Mahmud, H. Pota, and M. Hossain, "Dynamic stability of three-phase grid-connected photovoltaic system using zero dynamic design approach," *IEEE Journal of Photovoltaics,* vol. 2, pp. 564-571, 2012.Available at: https://doi.org/10.1109/jphotov.2012.2195551.

[27] H. M. Waseem, S. Jamwal, and M. Zaman, "Congestion control techniques in a computer network: A survey," *International Journal of Computer Applications,* vol. 111, pp. 7-10, 2015.Available at: https://doi.org/10.5120/19508-1112.

[28] A. Kulkarni and V. John, "Mitigation of lower order harmonics in a grid-connected single-phase PV inverter," *IEEE Transactions on Power Electronics,* vol. 28, pp. 5024-5037, 2013.Available at: https://doi.org/10.1109/tpel.2013.2238557.

[29] F.-J. Lin, K.-C. Lu, T.-H. Ke, B.-H. Yang, and Y.-R. Chang, "Reactive power control of three-phase grid-connected PV system during grid faults using Takagi–Sugeno–Kang probabilistic fuzzy neural network control," *IEEE Transactions on Industrial Electronics,* vol. 62, pp. 5516-5528, 2015.Available at: https://doi.org/10.1109/tie.2015.2407851.

[30] A. Timbus, M. Liserre, R. Teodorescu, and F. Blaabjerg, "Synchronization methods for three phase distributed power generation systems-An overview and evaluation," presented at the 2005 IEEE 36th Power Electronics Specialists Conference. IEEE, 2005.

[31] H. Khalfalla, S. Ethni, M. Al-Greer, V. Pickert, M. Armstrong, and V. T. Phan, "An adaptive proportional resonant controller for single phase PV grid connected inverter based on band-pass filter technique," presented at the 11th IEEE International Conference on Compatibility, Power Electronics and Power Engineering (CPE-POWERENG), 2017.

[32] M. Jahanbakhshi, B. Asaei, and B. Farhangi, "A novel deadbeat controller for single phase PV grid connected inverters," presented at the 23rd Iranian Conference on Electrical Engineering (ICEE), 2015.

[33] M. G. Villalva, J. R. Gazoli, and E. Ruppert Filho, "Comprehensive approach to modeling and simulation of photovoltaic arrays," *IEEE Transactions on Power Electronics,* vol. 24, pp. 1198-1208, 2009.Available at: https://doi.org/10.1109/tpel.2009.2013862.

[34] J. Mohammad and AfefFekih, "A comparison study between two sliding mode based controls for voltage sag mitigation in grid connected wind turbines," presented at the IEEE Conference on Control Applications (CCA) Part of 2015 IEEE Multi-Conference on Systems and Control September 21-23, 2015. Sydney, Australia, 2015.

[35] P. Giroux, G. Sybille, C. Osorio, and S. Chandrachood, "Detailed model of a 100-kW grid-connected PV array. Retrieved from https://www.mathworks.com/help/physmod/sps/examples/detailed-model-of-a-100-kw-grid-connected-pv-array.html?requestedDomain=www.mathworks.com," 2022.

[36] N. Zargari and G. Joos, "Performance investigation of a current-controlled voltage regulated PWM rectifier in rotating and stationary frames," *IEEE Transactions on Industrial Electronics,* vol. 42, pp. 396–401, 1995.

[37] A. J. Calderón, B. M. Vinagre, and V. Feliu, "Fractional order control strategies for power electronic buck converters," *Signal Processing,* vol. 86, pp. 2803-2819, 2006.Available at: https://doi.org/10.1016/j.sigpro.2006.02.022.